Passive microfluidic Pumping using coupled capillary/evaporation effects

N. Scott Lynn and David S. Dandy[*]

Department of Chemical and Biological Engineering
Colorado State University, Fort Collins, Colorado 80523

Supplementary Information

Summary of Model. A summary of the combined geometric/computational fluid dynamics (CFD) model is presented here, and additional details may be found in a previous publication.[1] The inlet and outlet reservoirs in this study, as well as in most LOC devices, have a length scale such that D_1, $D_2 < 3$ mm. For these systems, the Bond number can be calculated as $B_o = \rho g D_1^2 / 4\gamma_{lv} < 1$, such that surface tension forces dominant gravitational forces and it may be assumed that R_1 and R_2, the principal radii of curvature of an air/liquid interface, are not dependent on interfacial position. A stable open air/liquid meniscus situated in a reservoir can exist in either a complete or incomplete state, as shown in Fig. 2. The angles θ_1 and θ_2 are defined as the apparent contact angles between the reservoir floor and sidewalls, respectively. For a complete meniscus, the center of curvature is located at a point $(0, z_o)$, and it follows that $R_1 = R_2$. An incomplete meniscus has a primary radius of curvature R_1 extending from a point (r_o, z_o) to the meniscus in the r,z-plane, and a secondary radius of curvature R_2 extending from the line $r = 0$ to the average radial position of the meniscus in the r,θ-plane. An incomplete meniscus will exist in a stable form as shown in Fig. 2 when $2\alpha + \theta_1 + \theta_2 > \pi$, where 2α is the angle of intersection between the reservoir floor and sidewalls. There are two critical liquid

[*] To whom correspondence should be addressed. Email: dandy@colostate.edu, fax: 970.491.7369.

volumes at which the meniscus undergoes a discontinuous transition from a complete to incomplete state or *vice versa*. At a critical volume V_{ca}, the meniscus transition from a complete to incomplete state occurs under conditions such that $dV/dt < 0$ and the lowermost position of the air/liquid interface reaches the floor of the reservoir ($z_o = R_1$). At a critical volume V_{cb}, the meniscus transition from an incomplete to a complete state occurs conditions such that $dV/dt > 0$ where the distance between $r = 0$ and the position of the inner contact line approaches zero.

A simple model has been developed to calculate R_1, R_2, r_o, and z_o in a micro-reservoir, given values of D_1, D_2, H, θ_1, θ_2, and V. The shape of a meniscus situated in a reservoir may be estimated as a line of constant curvature R_1 symmetric along the z-axis intersecting the reservoir floor and sidewalls with θ_1 and θ_2, respectively. For specific values of R_1, the liquid volume V can then be calculated by integrating between the meniscus and the reservoir boundaries with respect to r, z, and θ. Relationships of R_1 versus V can then be used iteratively to calculate the shape of a meniscus given V for a reservoir with dimensions D_1, D_2, and H, and contact angles θ_1, and θ_2.

Calculated values of R_1, R_2, r_o, and z_o can then be used, together with knowledge of the temperature (T) and relative humidity (RH) for a system, to calculate instantaneous values of Q_e. Values of Q_e are calculated under the assumptions that the system is isothermal and isobaric, the gas phase within the reservoir is quiescent, and the mass fraction of water vapor is constant both along both the meniscus (x_{a1}) and the top of the reservoir at $z = H$ (x_{a2}), where x_{a1} can be calculated from Raoult's law and $x_{a2} = x_{a1}(1 - RH)$. For a given reservoir geometry, a minimum of 25 CFD simulations are used to solve the steady-state diffusion equation for the mass fraction of water vapor in the gas phase to obtain solutions of $x_a = x_a(r, z)$, where each simulation pertains

to a different liquid volume V. For each simulation the instantaneous evaporation rate can be calculated as

$$Q_e = \frac{-pM_w\mathcal{D}}{\rho RT}\int_A \frac{\partial x_a}{\partial \hat{n}} dA, \quad \textbf{(1s)}$$

Where M_w is the molecular weight of water, $\mathcal{D} = \mathcal{D}(T)$ is the binary diffusion coefficient of water vapor in air, R is the ideal gas constant, and A is the cross sectional area of integration normal to $\hat{n}$. Discrete values of Q_e versus V from individual CFD simulations are then fit to the following relationships:

$$\text{Complete meniscus} \quad Q_e = a_1 V^2 + a_2 V + a_3 \quad \textbf{(2s)}$$

$$\text{Incomplete meniscus} \quad Q_e = b_1 \log(V) + b_2 \log\left(\frac{V}{V_{res}}\right)^{b_3} \quad \textbf{(3s)}$$

where V_{res} is the total reservoir volume and the constants a_1, a_2, a_3, b_1, b_2, and b_3 are determined via (non)linear regression. The fits to discrete Q_e versus V data via Eqns. (2s) and (3s) result in values of $R^2 > 0.98$ for all cases.

Meniscus shape. Figure S1*A* displays calculated values of R_1 and R_2 for several reservoirs with varying upper and lower diameters, $H = 2.0$ mm, and contact angles $\theta_1 = 4°$ (glass) and $\theta_2 = 18°$ (oxidized PDMS), typical of experimental values in this study. Because these reservoirs contract in area as z increases ($D_2 < D_1$), the magnitude of R_1 (=R_2) will increase as V decreases for $V > V_{ca}$ for complete menisci, where the opposite is true for expanding reservoirs ($D_1 < D_2$). When evaporation causes the liquid volume in the reservoir to reach $V = V_{ca}$, the meniscus will rupture into an incomplete state due to the discontinuity between the initial air/liquid and eventual solid/liquid surface energies. For all reservoirs, values of R_1 and R_2 asymptote to zero and $D_1/2$, respectively, as the liquid volume V approaches zero, where $R_1 \propto V^{1/2}$ in the limit $V \to 0$ for all reservoirs, as seen in Fig. S1*A*. The Laplace pressure for menisci in reservoirs with low V will

thus scale as $\Delta p_i \propto V^{-1/2}$. Because the liquid pressure p_l in these reservoirs will be below atmospheric pressure—consistent with Eqn. (4)—flow in a common μFN connected by multiple reservoirs will always have flow directed toward the reservoir with smallest liquid volume, provided the meniscus in that reservoir is incomplete. The dependence of R_1 and R_2 on V is complicated and cannot be captured with simple analytical expressions. For incomplete menisci, R_1 will decrease with decreasing θ_1 and θ_2, and increasing D_1 for a given value of V, seen in Fig. S1*A*.

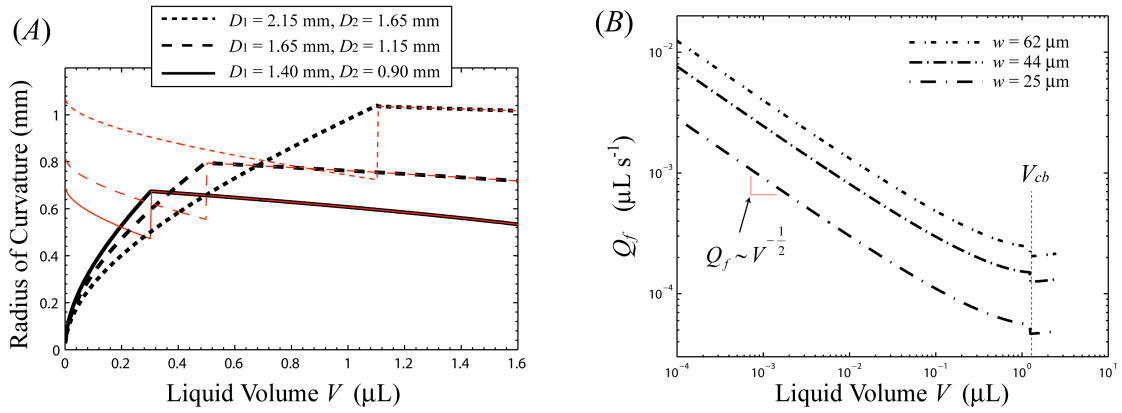

Figure S1. (*A*) The two primary radii of curvature, R_1 (black, thick line) and R_2 (red, thin line), plotted as a function of the liquid volume V contained in reservoirs with H = 2.0 mm and varying diameters. (*B*) Q_f vs. V calculated from Eqn. (2) for microchannels with h = 25 μm and varying width connected to an outlet reservoir with D_1 = 2.15 mm, D_2 = 1.65 mm, and H = 2.0 mm where the capillary forces associated with the inlet reservoir were neglected.

Considering a situation where a very large reservoir (negligible capillary forces) with arbitrarily large capacity feeds an outlet reservoir with a stable outlet meniscus with liquid volume V similar to that shown in Fig. 1*B*, one can solve for the instantaneous flow rates through the microchannel as a function of outlet reservoir liquid volume V by substituting Eqns. (3) and (4) into Eqn. (2). Figure S1*B* plots instantaneous values of Q_f as a function of V in this situation for three microchannels of different width. At the critical volume V_{cb} = 1.23 μL, the meniscus

transitions from an incomplete to a complete state and values of Q_f drop due to the sudden increase in R_2, as shown in Fig. 1*A*. For values of $V < 10^{-2}$ μL, the volumetric flow rate increases rapidly, scaling as $Q_f \propto V^{-1/2}$, which is consistent with the results shown in Fig. S1*A*. When the liquid volume is held constant, Q_f increases rapidly with increasing w, consistent with Eqns. (2) and (4).

Evaporation rate. The dependence of the evaporation rate on reservoir volume and contact angle is discussed in a previous study.[1] Although not shown here, there is a strong dependence of Q_e on θ_2 at large values of V, such that Q_e increases with decreasing θ_2 due to the increase in the interfacial area and average z-position of the meniscus. The dependence of Q_e on θ_1 and θ_2 is reduced substantially as $V \to 0$.

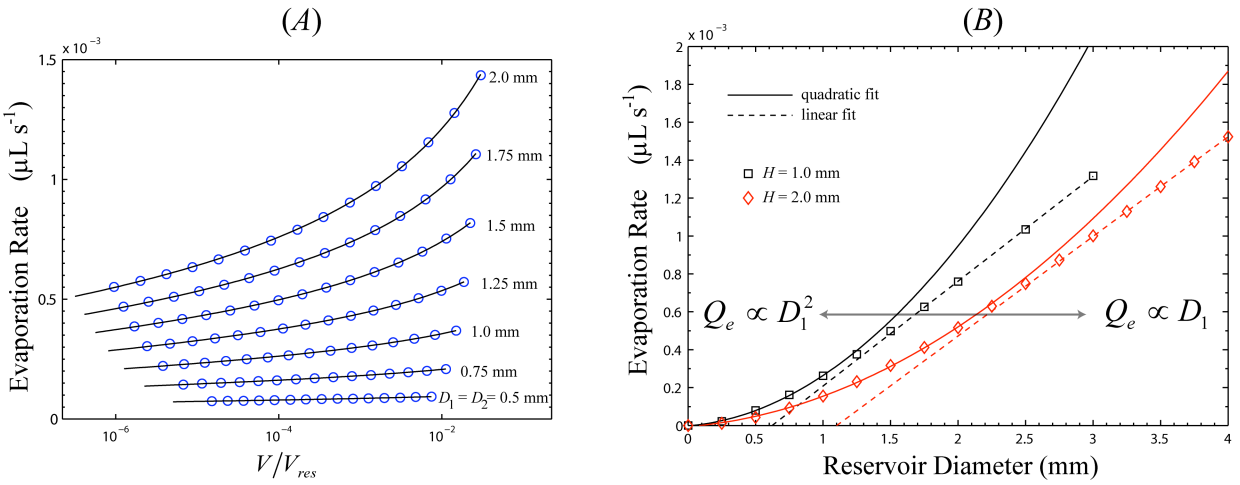

Figure S2. (*A*) Evaporation rate as a function of the normalized liquid reservoir volume for several cylindrical reservoir diameters with $H = 1.0$ mm. The symbols represent individual CFD simulations and the lines represent fits to Eqn. (3s). (*B*) Evaporation rate as a function of the reservoir diameter for reservoirs with $H = 1.0$ and 2.0 mm and $V/V_{res} = 10^{-4}$. The solid lines represent linear and quadratic fits to individual CFD simulations. Both figures pertain to reservoirs with $D_1 = D_2$ and external conditions of $T = 25$ °C and RH = 0.2.

In this study the focus is on the conditions typically associated with an outlet reservoir, where liquid volumes are below 0.1 μL and the meniscus exists in an incomplete state. Figure S2*A*

illustrates the evaporation rate as a function of V/V_{res} in reservoirs with height H = 1.0 mm for several diameters with the constraint $D_1 = D_2$. It can be seen that the dependence of Q_e on V is very weak as $V \rightarrow 0$ and $D_1 \rightarrow 0$. These results suggest that the overall diameter of the reservoir will have a significant effect on the overall flow rate of systems utilizing this passive pumping mechanism, provided that $V_{out}/V_{res} < 0.1$. Figure S2*B* displays the dependence of Q_e on the reservoir diameter (for cylindrical reservoirs) for systems with H = 1.0 and 2.0 mm. For all cases, Q_e increases with D_1; however, for smaller values of D_1, $Q_e \propto D_1^2$, while $Q_e \propto D_1$ for larger values of D_1, with the transition between the two scaling rates occurring at $D_1/H = O(1)$. This difference in scaling rates can be explained by examining the case for steady-state diffusion in a cylinder of diameter D_1 and height H with a small amount of water present along the bottom perimeter of the cylinder. In this case the mass fraction of water obeys $\nabla^2 x_a = 0$, with the bottom corner of the reservoir acting as a point source $x_a(D_1/2,0) = x_{a1}$, along with no flux conditions $dx_a/d\hat{n} = 0$ along the boundaries $r = a$ and $z = 0$. For the limiting case $D_1/H \ll 1$, the upper wall acts as a sink such that $x_a(r,H) = x_{a2}$, and the solution will resemble one-dimensional diffusion such that $\partial x_a/\partial r \approx 0$ and $dx_a/dz \approx (x_{a1} - x_{a2})/H$, thus Q_e will scale with the reservoir height as $Q_e \sim H^{-1}$. Furthermore, the differential area *dA* in Eqn. (1s) can be calculated along a plane of constant-*z*, thus $Q_e \sim rdrd\theta \propto D_1^2$. Conversely, for systems where $D_1/H \gg 1$, the system resembles diffusion from a thin ring of diameter D_1 into a semi-infinite medium. In this limiting case the evaporation rate will scale as the circumference of the meniscus, such that $Q_e \propto D_1$, which is consistent with several experimental studies concerning the evaporation rate from shallow wells.[2, 3] This scaling law can also be derived by examining the analogous situation regarding the electrical potential distribution due to a uniformly charged circular ring of diameter D_1.[4] These

two scaling laws are valid for all reservoirs where $V_{out}/V_{res} < 0.1$ and provide a good approximation for reservoirs with non-cylindrical geometries.

Prediction of time-dependent flow. Based on the results shown in Fig. S2, it is expected that both the geometries of the outlet reservoir and microchannel will control values of Q_f observed in laboratory systems consisting of a microchannel connecting inlet/outlet reservoirs composed of PDMS sidewalls and a glass floor. To predict the time-dependent flow occurring in these systems Eqn. (1) can be discretized using a first-order difference method as

$$V^{n+1} = V^n + \left(Q_e^n + Q_f^n + Q_{perm}^n\right)\Delta t, \qquad \textbf{(4s)}$$

where V^n is the liquid volume in a given reservoir at time $t = n\Delta t$. Given the shape of a meniscus in a reservoir, the evaporation rate $Q_e = Q_e(V)$ can be calculated using Eqn. (2s) or (3s) and Q_{perm} can be calculated using the liquid/PDMS interfacial area determined by the geometric model and a permeation flux of $J = 7\times10^{-6}$ kg m^{-2} s^{-1} taken from the experimental measurements of Randall *et al*. [5]. Using Eqns. (2), (3), and (4), $Q_f = Q_f(V)$ can be calculated using the relationship

$$\Delta p = \Delta p_{i,in} - \Delta p_{i,out} = \gamma_{in}\left(\frac{1}{R_{1,in}} + \frac{1}{R_{2,in}}\right) - \gamma_{out}\left(\frac{1}{R_{1,out}} + \frac{1}{R_{2,out}}\right). \qquad \textbf{(5s)}$$

Predictions of $v(t)$ were obtained by solving Eqn. (4s) for both reservoirs with a time step of Δt = 0.1 s, where at each time step values of Q_f^n, Q_e^n, and Q_{perm}^n were calculated from V_{in}^n and V_{out}^n. Because the tracer bead solutions used here are stabilized with a surfactant (tween-20) at a concentration of $C_s = 1.5\times10^{-7}$ M, decreases in both γ, θ_1, and θ_2 are expected over time as the surfactant concentration increases in both reservoirs due to evaporative effects. The surfactant concentration in the reservoirs can be calculated utilizing Eqn. (4s) along with

$$C_{s,out}^{n+1} = \left(M_{s,out}^{n} + Q_f^n C_{s,in}^n \Delta t\right) / V_{out}^n \,, \qquad \textbf{(6s)}$$

where M_s is the molar mass of surfactant in each reservoir. From the results of Niño *et al.*,[6] changes in the interfacial tension with surfactant concentration can be accounted for via $\gamma = \alpha_1 \log(C_s) + \alpha_2$ for the range 4×10^{-7} M < C_s < $C_{s,crit}$, where α_1 = -21.6 g s^{-2} and α_2 = -65.8 g s^{-2}; γ = 73 g s^{-2} for the range $C_s < 4\times10^{-7}$ M; and γ = 33 g s^{-2} for the range $C_s > C_{s,crit}$, where the critical micelle concentration (CMC) for tween-20 in water is $C_{s,crit} = 2.5\times10^{-5}$ M. For the outlet reservoir, C_s is predicted to exceed the CMC in the outlet reservoir within 30 seconds for all cases in this study, after which γ_{out}, $\theta_{1,out}$ and $\theta_{2,out}$ are not expected to change over time.

Laboratory measurements of the contact angles for the reservoir floor and sidewalls are accomplished utilizing the techniques developed in a previous study.[1] Briefly, this measurement is done by observing the position of the inner contact line along the floor of a reservoir over time as the effects of evaporation reduce the liquid volume in a reservoir with known geometry. An iterative process matching laboratory observations to predictions from the geometric model of the contact line position then provides accurate values of θ_1 and θ_2 for a wide range of reservoir geometries and external conditions. For aqueous solutions with surfactant concentrations well above the CMC of $C_s = 8\times10^{-5}$ M, the contact angles for the outlet reservoir were measured to be $\theta_{1,out} = 4.2 \pm 1.0°$ and $\theta_{2,out} = 18.2 \pm 2.5°$. In contrast, for dilute aqueous solutions with $C_s = 1.5\times10^{-7}$ M, contact angles were $\theta_{1,in} = 13 \pm 5.4°$ and $\theta_{2,in} = 49.6 \pm 4.7°$. These values are used as inputs to the geometric model discussed above to establish predictions for R_1 and R_2 as a function of V_{out}. Because the capillary forces associated with the inlet reservoir are small ($R_{1,in}$,$R_{2,in}$ » $R_{1,out}$) and $C_{s,in}$ does not increase appreciably until close to reservoir dry out, it is reasonable to neglect variations in $\theta_{1,in}$ and $\theta_{2,in}$ with time.

Regarding variation of Q_e with temperature, values of T and RH are measured at the onset and completion of an experiment. For predictive reasons it is assumed that any changes are linear with time and values of Q_e are calculated accordingly. With respect to the environment surrounding the reservoir, according to Eqn. (1s) the evaporation rate scales as $Q_e \propto x_{a1}\mathcal{D}T^{-1}$, independent of the reservoir volume.

References

1. N. S. Lynn, C. S. Henry and D. S. Dandy, *Lab Chip*, 2009, **9**, 1780-1788.
2. C. T. Chen, F. G. Tseng and C. C. Chieng, *Sensor Actuat a-Phys*, 2006, **130**, 12-19.
3. L. R. van den Doel and L. J. van Vliet, *Appl Optics*, 2001, **40**, 4487-4500.
4. P. Zhu, *J Electrostat*, 2005, **63**, 1035-1047.
5. G. C. Randall and P. S. Doyle, *P Natl Acad Sci USA*, 2005, **102**, 10813-10818.
6. R. R. Nino and J. M. R. Patino, *J Am Oil Chem Soc*, 1998, **75**, 1241-1248.